

Density Functional Study of Butadiyne to Butatrienylidene Isomerization in $[\text{Ru}(\text{HC}\equiv\text{CC}\equiv\text{CH})(\text{PMe}_3)_2(\text{Cp})]^+$

Francesco Creati, Cecilia Coletti, and Nazzareno Re*

Dipartimento di Scienze del Farmaco, Università G. D'Annunzio, Via dei Vestini, 31, I-66100 Chieti, Italy

Received August 20, 2009

The butadiyne to butatrienylidene isomerization in $[\text{Ru}(\text{HC}\equiv\text{CC}\equiv\text{CH})(\text{PMe}_3)_2(\text{Cp})]^+$ has been investigated by density functional calculations. Several possible minima have been identified on the potential energy surface for the coordinated C_4H_2 moiety, and a few plausible isomerization mechanisms have been analyzed by a DFT approach. The butatrienylidene complex has been found to be more stable than the butadiyne adduct by $-13.1 \text{ kcal mol}^{-1}$ in enthalpy and is the thermodynamically most stable species on the potential energy surface. The energetically most favorable isomerization pathway has been found to initially follow the same pathway experimentally and theoretically characterized for the simpler alkyne rearrangement on a d^6 metal fragment, i.e. a 1,2-hydrogen shift passing through an agostic intermediate, and leading to a ethynyl vinyl intermediate, for which an activation enthalpy of $23.1 \text{ kcal mol}^{-1}$ (activation free energy of $20.8 \text{ kcal mol}^{-1}$) was found. The isomerization then proceeds through a proton migration from the C_β to the terminal C_δ atom occurring through deprotonation of the ethynyl vinylidene, leading to a butadiynyl complex which is then reprotonated to the final butatrienylidene product, with an overall activation energy of $17.4 \text{ kcal mol}^{-1}$ (activation free energy of $19.6 \text{ kcal mol}^{-1}$).

1. Introduction

Unsaturated carbenes, $:\text{C}=(=\text{C})_n=\text{CR}_2$,¹ are extremely reactive species which can be most conveniently generated by special gas-phase techniques, such as flash vacuum pyrolysis or photolysis of suitable precursors,² although shorter terms have been prepared by conventional liquid-phase synthesis.³ They are all extremely unstable species with short lifetimes, even if longer chain cumulenes are relatively more stable, and have been trapped in cold matrices⁴ and detected in interstellar cold molecular clouds.⁵ The stabilization of these

unsaturated cumulenes by coordination to a transition-metal center is well established and constitutes a field of intense current activity in organometallic chemistry.⁶ This stabilization is achieved through the donation of the electron lone pair on the terminal carbon atom to an empty metal d orbital and the simultaneous back-donation from a filled metal d_π orbital to empty cumulene π^* system orbitals.⁷ The resulting unsaturated $[\text{L}_m\text{M}] \text{C}=(=\text{C})_n=\text{CR}_2$ complexes have recently received much attention because they can be potential precursors of molecular wires of interest in the field of novel optoelectronic materials⁸ and can also provide multifaceted reactive sites of interest in organic synthesis.^{6,9}

The first members of this series, the transition-metal vinylidene and allenylidene complexes $[\text{L}_m\text{M}] = \text{C}=\text{CR}_2$ and $[\text{L}_m\text{M}] = \text{C}=\text{C}=\text{CRR}'$, respectively, have been known since the early 1970s,¹⁰ and their chemistry has developed

*To whom correspondence should be addressed. Tel: +39 0871 355 4603. Fax: +39 0871 355 4614. E-mail: nre@unich.it.

(1) (a) Stang, P. J. *Chem. Rev.* **1978**, *78*, 383. Maluendes, S. A.; McLean, A. D. *Chem. Phys. Lett.* **1992**, *200*, 511. (b) Brandsma, L. *Best Synthetic Methods: Acetylenes, Allenes and Cumulenes*; Elsevier: Amsterdam, 2003.

(2) (a) Vrtilek, J. M.; Gottlieb, C. A.; Gottlieb, E. W.; Killian, T. C.; Thaddeus, P. *Astrophys. J.* **1990**, *364*, L53. (b) Killian, T. C.; Vrtilek, J. M.; Gottlieb, C. A.; Gottlieb, E. W.; Thaddeus, P. *Astrophys. J.* **1990**, *365*, L89. (c) Travers, M. J.; Chen, W.; Novick, S. E.; Vrtilek, J. M.; Gottlieb, C. A.; Thaddeus, P. *J. Mol. Spectrosc.* **1996**, *180*, 75.

(3) (a) Stang, P. J.; Fisk, T. E. *J. Am. Chem. Soc.* **1979**, *101*, 4772. (b) le Noble, W. J.; Basak, S.; Srivastava, S. *J. Am. Chem. Soc.* **1981**, *103*, 4638.

(c) Stang, P. J.; Learned, A. E. *J. Chem. Soc., Chem. Commun.* **1988**, 301.

(4) (a) Maier, G.; Preiss, T.; Reisenauer, H. P.; Hess, B. A., Jr.; Schaad, L. J. *J. Am. Chem. Soc.* **1994**, *116*, 2014. (b) Maier, G.; Preiss, T.; Reisenauer, H. P. *Chem. Ber.* **1994**, *127*, 779.

(5) (a) Kaiser, R. I. *Chem. Rev.* **2002**, *102*, 1309–1358. Herbst, E. *Chem. Soc. Rev.* **2001**, *30*, 168. (b) Woods, P. M.; Millar, T. J.; Herbst, E.; Zijlstra, A. A. *Astron. Astrophys.* **2003**, *402*, 189.

(6) (a) Bruce, M. I. *Chem. Rev.* **1998**, *98*, 2797. (b) Touchard, D.; Dixneuf, P. H. *Coord. Chem. Rev.* **1998**, *178*, 409. (c) Cadierno, V.; Gamasa, M. P.; Gimeno, J. *Eur. J. Inorg. Chem.* **2001**, *571*. (d) Bruce, M. I. *Coord. Chem. Rev.* **2004**, *248*, 15. (e) Cadierno, V.; Gamasa, M. P.; Gimeno, J. *Chem. Rev.*, in press.

(7) (a) Re, N.; Sgammellotti, A.; Floriani, C. *Organometallics* **2000**, *19*, 1115. (b) Marrone, A.; Re, N. *Organometallics* **2002**, *21*, 3562. (c) Marrone, A.; Coletti, C.; Re, N. *Organometallics* **2004**, *23*, 4952. (d) Auger, N.; Touchard, D.; Rigaut, S.; Halet, J.-F.; Saillard, J.-Y. *Organometallics* **2003**, *22*, 1638.

(8) (a) Bartik, T.; Bartik, B.; Brady, M.; Dembinski, R.; Gladysz, J. A. *Angew. Chem., Int. Ed. Engl.* **1996**, *35*, 414. (b) Coat, F.; Lapinte, C. *Organometallics* **1996**, *15*, 477. (c) Stang, P. J.; Tykwienski, R. *J. Am. Chem. Soc.* **1992**, *114*, 4411. (d) Long, N. J. *Angew. Chem., Int. Ed. Engl.* **1995**, *34*, 21. (e) Whittal, I. R.; McDonagh, A. M.; Humphrey, M. G.; Samoc, M. *Adv. Organomet. Chem.* **1999**, *43*, 349.

(9) *Metal Vinylidenes and Allenylidenes in Catalysis: From Reactivity to Applications in Synthesis*; Bruneau, C., Dixneuf, P. H., Eds.; Wiley-VCH: Weinheim, Germany, 2008.

(10) (a) King, R. B.; Saran, M. S. *J. Am. Chem. Soc.* **1972**, *94*, 1784. (b) Fischer, E. O.; Kalder, H. J.; Frank, A.; Köhler, F. H.; Huttner, G. *Angew. Chem., Int. Ed. Engl.* **1976**, *15*, 623.

rapidly in the past three decades due to their application in organic reactions and catalysis.^{11,12}

A wide range of vinylidene and allenylidene complexes has been synthesized and characterized with a variety of metals, among which those with Ru(II) constitute the most extended group, and these have been recognized as key active intermediates in catalytic selective transformation of alkynes promoted by cationic ruthenium catalysts.¹²

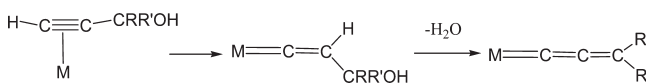
Vinylidenes are tautomers of 1-alkynes and are formed by a formal 1,2-shift of the alkyne hydrogen from C₁ to C₂ (see Scheme 1).¹³ Also, one of the most common synthetic approaches to the preparation of metal allenylidenes involves the use of propargylic alcohols, which first undergo an alkynyl–vinylidene rearrangement followed by the elimination of a water molecule (see Scheme 2).¹⁴

The alkyne to vinylidene rearrangement in the coordination sphere of a transition metal is therefore a key step in the entry to vinylidenes and allenylidene chemistry and has attracted much interest from both an experimental^{13,15–17} and a theoretical point of view.¹⁸ Theoretical calculations have clearly shown that, while the formation of vinylidene from free acetylene is a strongly endothermic (44–47 kcal mol⁻¹) process,^{19,20} the relative energies of the two isomers

Scheme 1. η^2 -Alkyne \rightarrow η^1 -Vinylidene Isomerization



Scheme 2. Reaction Pathway for the Synthesis of Metal Allenylidenes from Propargylic Alcohols



change dramatically in the coordination sphere of several transition metals and, indeed, metal vinylidenes are stable complexes and may be more stable than the corresponding acetylene isomers.¹⁸ Two different pathways have been proposed for the metal-assisted isomerization of 1-alkyne to vinylidene (Scheme 3): (i) an intramolecular 1,2-hydrogen shift from C_α to C_β with a concomitant detachment of C_β from the metal (paths 1A and 1B) and (ii) an oxidative addition of the coordinated 1-alkyne to give a hydrido alkynyl complex which then isomerizes by a 1,3-hydrogen shift from the metal to C_β (path 2).^{13,18}

In the last decade also a few cumulene complexes have been reported with four or more carbon atoms.^{21,22} Butatrienyldene metal complexes have been proposed as plausible intermediates,^{21a,b} and only two have been recently isolated and structurally characterized by X-ray methods.^{21c–e} Very few pentatetraenyldene metal complexes have been synthesized and fully characterized in the last few years.²² An heptahexaenyldene complex of chromium pentacarbonyl has been recently isolated and spectroscopically characterized and is up to now the longest isolated metal cumulenyldene complex.²³

This increasing activity toward longer chain cumulynidene complexes has also stirred interest in the stabilization of longer chain cumulenes by metal centers and in the possible isomerization mechanisms for their formation from stable unsaturated organic molecules.^{24–27}

- (11) (a) Bruce, M. I.; Swincer, A. G. *Adv. Organomet. Chem.* **1983**, *22*, 59. (b) Bruce, M. I. *Chem. Rev.* **1991**, *91*, 197 and references therein.
- (12) (a) Katayama, H.; Ozawa, F. *Coord. Chem. Rev.* **2004**, *248*, 1703. (b) Trost, B. M.; Frederiksen, M. U.; Rudd, M. T. *Angew. Chem., Int. Ed.* **2005**, *44*, 6630. (c) Bruneau, C.; Dixneuf, P. H. *Angew. Chem., Int. Ed.* **2006**, *45*, 2176.
- (13) (a) Puerta, M. C.; Valerga, P. *Coord. Chem. Rev.* **1999**, *193*–195, 977–1025. (b) Wakatsuki, Y. J. *Organomet. Chem.* **2004**, *689*, 4092–4109.
- (14) (a) Selegue, J. P. *Organometallics* **1982**, *1*, 217. (b) Nickias, P. N.; Selegue, J. P.; Young, B. A. *Organometallics* **1988**, *7*, 2248.
- (15) (a) Wolf, J.; Werner, H.; Serhadli, O.; Ziegler, M. L. *Angew. Chem., Int. Ed. Engl.* **1983**, *22*, 414. (b) Werner, H.; Höhn, A. J. *Organomet. Chem.* **1984**, *272*, 105. (c) García-Alonso, F. J.; Höhn, A.; Wolf, J.; Otto, H.; Werner, H. *Angew. Chem., Int. Ed. Engl.* **1985**, *24*, 406. (d) Dziallas, M.; Werner, H. *J. Chem. Soc., Chem. Commun.* **1987**, 852. (e) Bianchini, C.; Masi, D.; Meli, A.; Peruzzini, M.; Ramírez, J. A. *Organometallics* **1989**, *8*, 2179. (f) Bianchini, C.; Peruzzini, M.; Vacca, A.; Zanobini, F. *Organometallics* **1991**, *10*, 3697.
- (16) (a) Bruce, M. I.; Wong, F. S.; Skelton, B. W.; White, A. H. *J. Chem. Soc., Dalton Trans.* **1982**, 2203. (b) Bullock, R. M. *J. Chem. Soc., Chem. Commun.* **1989**, 165. (c) Cadierno, V.; Gamasa, M. P.; Gimeno, J.; Pérez-Carreño, E.; García-Granda, S. *Organometallics* **1999**, *18*, 2821. (d) Cadierno, V.; Gamasa, M. P.; Gimeno, J.; González-Bernardo, C.; Pérez-Carreño, E.; García-Granda, S. *Organometallics* **2001**, *20*, 5177. (e) Bassetti, M.; Cadierno, V.; Gimeno, J.; Pasquini, C. *Organometallics* **2008**, *27*, 5009.
- (17) (a) de Los Ríos, I.; Jiménez-Tenorio, M.; Puerta, M. C.; Valerga, P. *J. Am. Chem. Soc.* **1997**, *119*, 6529. (b) Bustelo, E.; Jiménez-Tenorio, M.; Puerta, M. C.; Valerga, P. *Organometallics* **1999**, *18*, 4563. (c) Aneetha, H.; Jiménez-Tenorio, M.; Puerta, M. C.; Valerga, P. *Organometallics* **2003**, *22*, 2001. (d) Bustelo, E.; Carb, J. J.; Lledos, A.; Mereiter, K.; Puerta, M. C.; Valerga, P. *J. Am. Chem. Soc.* **2003**, *125*, 3311.
- (18) (a) Silvestre, J.; Hoffmann, R. *Helv. Chim. Acta* **1985**, *68*, 1461. (b) Wakatsuki, Y.; Koga, N.; Yamazaki, H.; Morokuma, K. *J. Am. Chem. Soc.* **1994**, *116*, 8105. (c) Wakatsuki, Y.; Koga, N.; Werner, H.; Morokuma, K. *J. Am. Chem. Soc.* **1997**, *119*, 360. (d) Stegmann, R.; Frenking, G. *Organometallics* **1998**, *17*, 2089. (e) Pérez-Carreño, E.; Paoli, P.; Ienco, A.; Mealli, C. *Eur. J. Inorg. Chem.* **1999**, 1315. (f) Tokunaga, M.; Suzuki, T.; Koga, N.; Fukushima, T.; Horiuchi, A.; Wakatsuki, Y. *J. Am. Chem. Soc.* **2001**, *123*, 11917. (g) De Angelis, F.; Sgamellotti, A.; Re, N. *Organometallics* **2002**, *21*, 2715. (h) De Angelis, F.; Sgamellotti, A.; Re, N. *Organometallics* **2002**, *21*, 5944. (i) De Angelis, F.; Sgamellotti, A.; Re, N. *Dalton Trans.* **2005**, 3225. (j) De Angelis, F.; Sgamellotti, A.; Re, N. *Organometallics* **2007**, *26*, 5285. (k) Vastine, B. A.; Hall, M. B. *Organometallics* **2008**, *27*, 4325.
- (19) (a) Chen, Y.; Jonas, D. M.; Kinsey, J. L.; Field, R. W. *J. Chem. Phys.* **1989**, *91*, 3976. (b) Erwin, K. M.; Gronert, S.; Barlow, S. E.; Gilles, M. K.; Harrison, A. G.; Bierbaum, V. M.; DePuy, C. H.; Lineberger, W. C.; Ellison, G. B. *J. Am. Chem. Soc.* **1990**, *112*, 5750.
- (20) (a) Gallo, M. M.; Hamilton, T. P.; Schaefer, H. F. *J. Am. Chem. Soc.* **1990**, *112*, 8714. (b) Jensen, J. H.; Morokuma, K.; Gordon, M. S. *J. Chem. Phys.* **1994**, *110*, 1981.

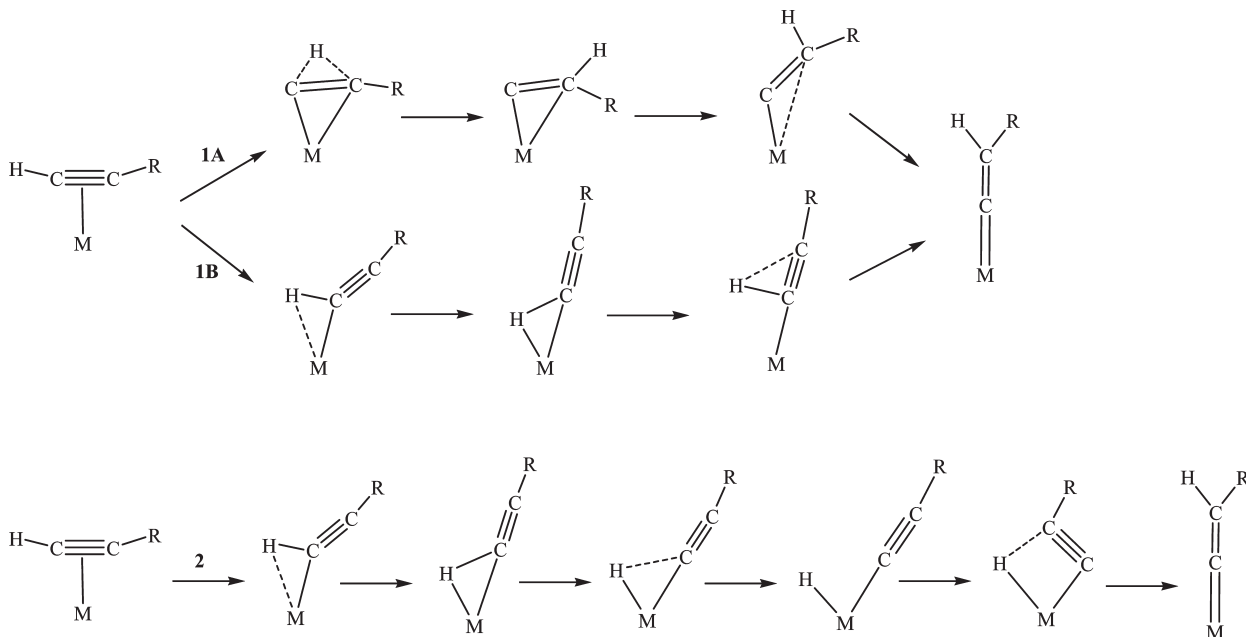
- (21) (a) Lomprey, J. R.; Selegue, J. P. *Organometallics* **1993**, *12*, 616. (b) Bruce, M. I.; Hinterding, P.; Low, P. J.; Skelton, B. W.; White, A. H. *J. Chem. Soc., Chem. Commun.* **1996**, 1009. (c) Ilg, K.; Werner, H. *Angew. Chem., Int. Ed. Engl.* **2000**, *39*, 1632. (d) Ilg, K.; Werner, H. *Chem. Eur. J.* **2002**, *8*, 2812. (e) Venkatesan, K.; Fernández, F. J.; Blaque, O.; Fox, T.; Alfonso, M.; Schmalke, H. W.; Berke, H. *Chem. Commun.* **2003**, 2006.

- (22) (a) Touchard, D.; Haquette, P.; Daridor, A.; Toupet, L.; Dixneuf, P. H. *J. Am. Chem. Soc.* **1994**, *116*, 11157. (b) Peron, D.; Romero, A.; Dixneuf, P. H. *Organometallics* **1995**, *14*, 3319. (c) Lass, R. W.; Steinert, P.; Wolf, J.; Werner, H. *Chem. Eur. J.* **1996**, *2*, 19. (d) Kovacic, I.; Laubender, M.; Werner, H. *Organometallics* **1997**, *16*, 5607. (e) Roth, G.; Fischer, H. *Organometallics* **1996**, *15*, 1139. (f) Roth, G.; Fischer, H. *Organometallics* **1996**, *15*, 5766. (g) Roth, G.; Fischer, H.; Meyer-Friedrichsen, T.; Heck, J.; Houbrechts, S.; Persons, A. *Organometallics* **1998**, *17*, 1511.

- (23) Dede, M.; Drexler, M.; Fischer, H. *Organometallics* **2007**, *26*, 4294–4299.

- (24) (a) Bruce, M. I.; Hinterding, P.; Ke, M.; Low, P. J.; Skelton, B. W.; White, A. H. *Chem. Commun.* **1997**, 715. (b) Bruce, M. I.; Hinterding, P.; Low, P. J.; Skelton, B. W.; White, A. H. *J. Chem. Soc., Dalton Trans.* **1998**, 467. (c) Bruce, M. I.; Ellis, B. G.; Skelton, B. W.; White, A. H. *J. Organomet. Chem.* **2005**, 690, 1772.
- (25) (a) Winter, R. F.; Hornung, F. M. *Organometallics* **1997**, *16*, 4248. (b) Winter, R. F.; Hartmann, S.; Záliš, S.; Klinkhammer, K. W. *Dalton Trans.* **2003**, 2342. (c) Hartmann, S.; Winter, R. F.; Sarkar, B.; Lissner, F. *Dalton Trans.* **2004**, 3273.

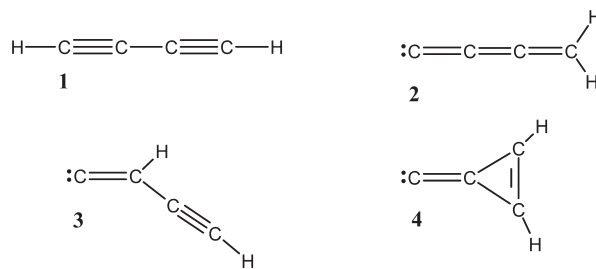
- (26) (a) Haquette, P.; Touchard, D.; Toupet, L.; Dixneuf, P. *J. Organomet. Chem.* **1998**, 565, 63. (b) Guillaume, V.; Thominot, P.; Coat, F.; Mari, A.; Lapinte, C. *J. Organomet. Chem.* **1998**, 565, 75.
- (27) Yamauchi, Y.; Yuki, M.; Tanabe, Y.; Miyake, Y.; Inada, Y.; Uemura, S.; Nishibayashi, Y. *J. Am. Chem. Soc.* **2008**, *130*, 2908.

Scheme 3. Alternative Pathways for the η^2 -Alkyne \rightarrow η^1 -Vinylidene Isomerization

Following the pioneering work of Selegue and Bruce,^{21a,b} in the last few years several groups have reported a series of reactions that have been rationalized as proceeding via butatrienylidene intermediates, formed in situ from the reaction of 1,3-butadiynes with electron-rich Ru(II) metal complexes with a labile ligand,^{24–27} such as $[\text{Ru}(\text{thf})(\text{PR}_3)_2\text{Cp}]^+$,²⁴ *cis*- $\text{RuCl}_2(\text{dppm})_2$,²⁵ and *cis*- $\text{RuCl}_2(\text{dppe})_2$.²⁶ However, due to their excessive reactivity, the corresponding $[\text{Ru}(=\text{C}=\text{C}=\text{C}=\text{CH}_2)(\text{PR}_3)_2\text{Cp}]^+$, $[\text{cis-Ru}(=\text{C}=\text{C}=\text{C}=\text{CH}_2)-(\text{dppm})_2\text{Cl}]^+$, and $[\text{cis-Ru}(=\text{C}=\text{C}=\text{C}=\text{CH}_2)(\text{dppe})_2\text{Cl}]^+$ butatrienylidene complexes have never been isolated along this route because they easily add a nucleophile at the C_γ carbon, leading—depending on the nucleophile—to functionalized allenylidenes or ethynyl complexes.

A butatrienylidene complex, $[\text{Mn}(=\text{C}=\text{C}=\text{C}=\text{CH}_2)-(\text{dmpe})(\text{C}_5\text{H}_4\text{R})]^+$ ($\text{R} = \text{H}, \text{Me}$), could be observed and characterized by NMR spectroscopy in solution only by reacting a tin-substituted 1,3-butadiyne, $\text{Me}_3\text{SnC}\equiv\text{CC}\equiv\text{CSnMe}_3$, with a Mn(I) d⁶ synthon and deprotecting the terminal SnMe₃ groups of the initially formed, more stable $[\text{Mn}(=\text{C}=\text{C}=\text{C}(\text{SnMe}_3)_2)(\text{dmpe})(\text{C}_5\text{H}_4\text{R})]^+$ complex.^{21e,28}

The formation of butatrienylidene through a formal 1,4-hydrogen shift of 1,3-butadiyne on a Ru(II) complex is particularly interesting from both experimental and theoretical points of view, as this reaction is a prototypical example of the activation of polyynes on transition metal centers—the most direct route to the preparation of metallacumulenes, carbon-chain-bridged dinuclear complexes, and molecular wires—and its detailed mechanism has not yet been clarified. Previous computational studies of the C₄H₂ potential energy surface²⁹ have identified the 1,3-butadiyne **1** as the most stable isomer with the butatrienylidene species **2** 50–55 kcal mol⁻¹ above and the remaining isomers **3–5** still higher in

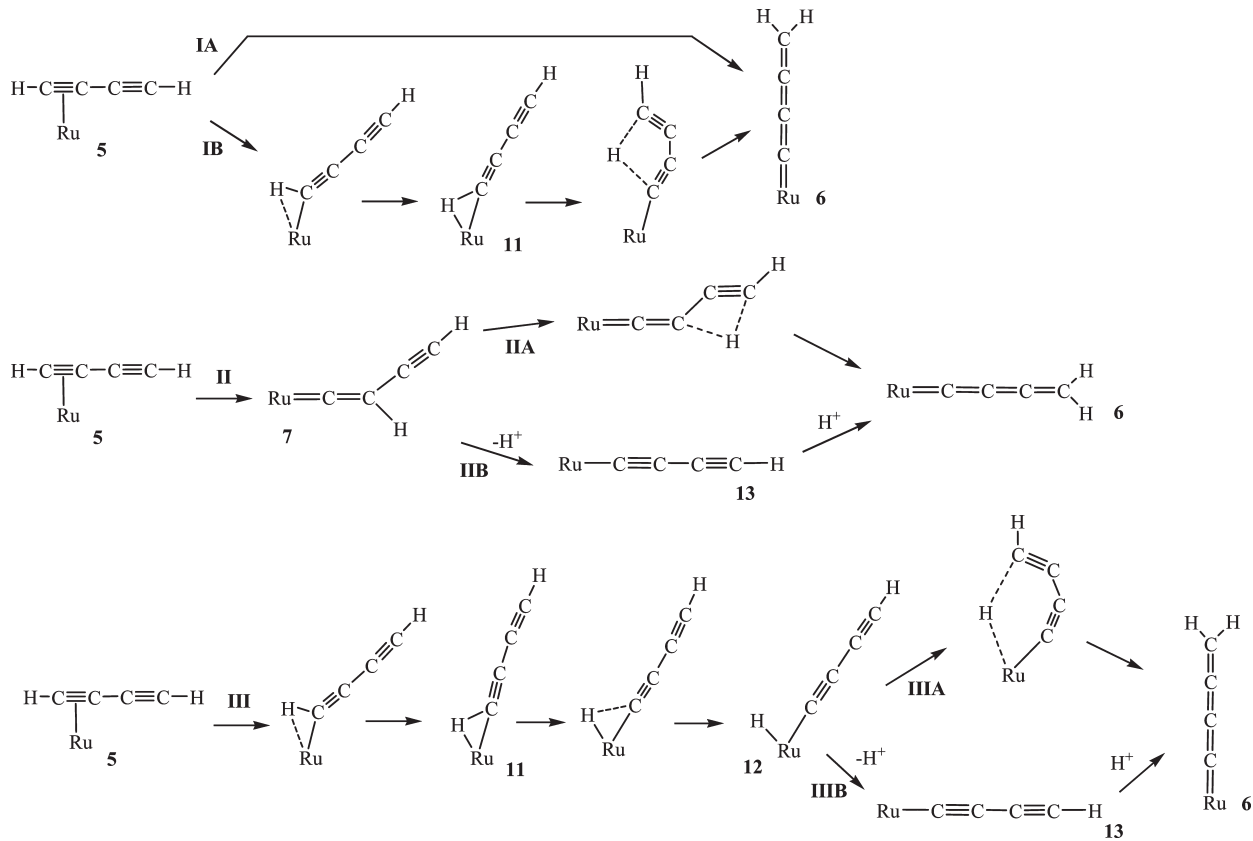
Chart 1. Most Stable Isomers of the C₄H₂ Moiety

energy (see Chart 1), while the formation of butatrienylidene complexes shows that this energy order may change when the C₄H₂ moiety is coordinated to a metal center.

Several pathways have been suggested for the butadiyne to butatrienylidene tautomerization (see Scheme 4): (i) a direct 1,4-hydrogen shift (paths IA and IB), (ii) a two-step pathway with an initial 1,2-hydrogen shift leading to an ethynylvinylidene intermediate, which then further rearranges to the final butatrienylidene complex through either an intramolecular 1,3-hydrogen shift or a deprotonation of the vinylidene hydrogen to give a butadiynyl complex which is then reprotonated on the terminal C_δ atom (paths IIA and IIB), and (iii) an oxidative addition of the coordinated 1,3-butadiyne to give a hydrido–butadiynyl complex which then further isomerizes through either a direct intramolecular 1,5-hydrogen shift from the metal to C_δ or a deprotonation of the metal-bound hydrogen followed by a reprotonation of the butadiynyl ligand on the terminal C_δ atom (paths IIIA and IIIB).²⁴ The proton migration step from Ru to C_δ in the product of the butadiyne oxidative addition in path IIIB has been already observed for the hydrido alkynyl intermediates isolated in the alkyne to vinylidene isomerization on electron-rich Ru(II) fragments, such as $[\text{Ru}(\text{L-L})(\text{Cp}^*)]^+$, where L-L is a bidentate diphosphine or two monodentate phosphines,¹⁷ whereas the proton migration from C_β to C_δ in the ethynyl vinylidene intermediate in path IIB has been suggested by the relatively high acidity of vinylidenes.²⁴

(28) (a) Konkol, M.; Steiborn, D. *J. Organomet. Chem.* **2006**, 691, 2839. (b) Venkatesan, K.; Blaque, O.; Fox, T.; Alfonso, M.; Schmalle, H. W.; Berke, H. *Organometallics* **2006**, 23, 4661.

(29) (a) Dykstra, C. E.; Parsons, C. A.; Oates, C. L. *J. Am. Chem. Soc.* **1979**, 101, 1962. (b) Collins, C. L.; Meredith, C.; Yamaguchi, Y.; Schaefer, H. F., III *J. Am. Chem. Soc.* **1992**, 114, 8694. (c) Mabry, J.; Johnson, R. P. *J. Am. Chem. Soc.* **2002**, 124, 6497.

Scheme 4. Possible Pathways Proposed for the η^2 -Butadiyne \rightarrow η^1 -Butatrienylidene Isomerization

In this paper we report extensive DFT calculations on the isomerization of the $[\text{Ru}(\eta^2\text{-HC}\equiv\text{CC}\equiv\text{CH})(\text{PMe}_3)_2(\text{Cp})]^+$ butadiyne complex to the corresponding $[\text{Ru}(=\text{C}\equiv\text{C}\equiv\text{CH}_2)(\text{PMe}_3)_2(\text{Cp})]^+$ tautomer.

We performed DFT calculations in order to compute the geometries and the relative stabilities of the main stationary points of the potential energy surface for the butadiyne rearrangement on the Ru(II) center and considered all the possible pathways in Scheme 4, pointing out the most favored pathway for the butadiyne to butatrienylidene isomerization in the metal coordination sphere.

2. Background

Although, to the best of our knowledge, no calculation has been performed on the metal-catalyzed butadiyne to butatrienylidene tautomerization, the metal-catalyzed alkyne to vinylidene isomerization has been thoroughly investigated from a theoretical point of view.¹⁸ It has been found that the alkyne to vinylidene isomerization pathway depends on the electron configuration of the metal center. Experimental and theoretical results indicate that the acetylene rearrangement on a d⁶ metal fragment, such as Mn(I) or Ru(II), proceeds via a 1,2-hydrogen shift, path 1 in Scheme 3, the mechanism involving oxidative addition being difficult due to a relatively unfavorable change from a d⁶ to a d⁴ metal configuration;¹⁶ the only exception to this rule is the isomerization of 1-alkynes on the highly electron rich $[(\text{Cp}^*)(\text{L-L})\text{Ru}]^+$ fragment ($\text{L-L} = (\text{PR}_3)_2$, dippe), for which a hydrido alkynyl complex has been isolated and structurally characterized.¹⁷

A different situation has been found for the alkyne rearrangement on a d⁸ metal fragment, such as Co(I), Rh(I), or Ir(I), for which the mechanism involving the initial alkyne

oxidative addition (path 2) is preferred due to a more favorable d⁸ to d⁶ metal change. Indeed, there are several examples of 1-alkyne rearrangements on Rh(I), Ir(I), and Co(I) metal fragments where hydrido alkynyl intermediates have been detected and even isolated.¹⁵ Moreover, ab initio calculations on the rhodium(I) d⁸ $[\text{Cl}(\text{PH}_3)_2\text{Rh}(\text{HC}\equiv\text{CH})]$ complex showed that in this case the rearrangement proceeds through a stable hydrido alkynyl intermediate which then leads to the vinylidene complex.^{18j}

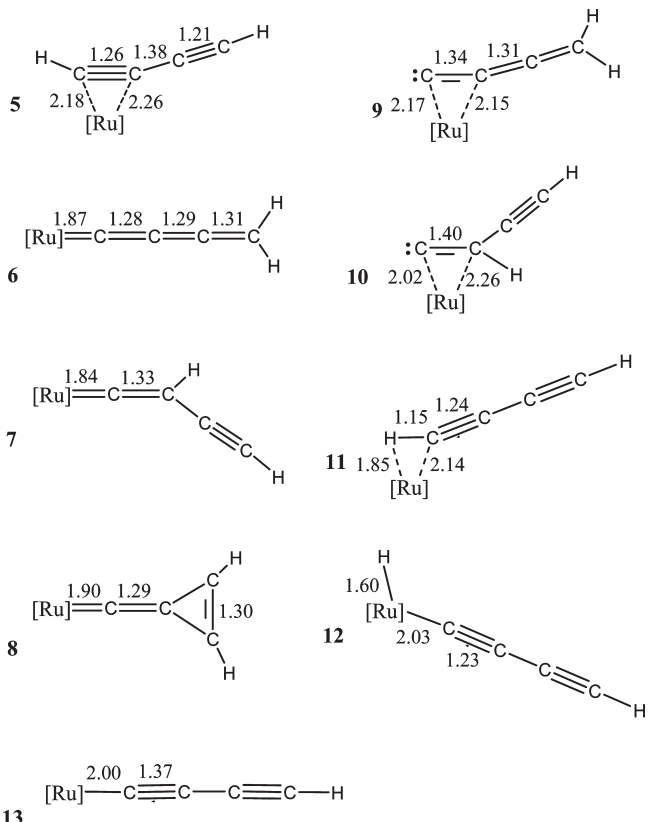
Theoretical investigations have brought important contributions to clarify the details of the 1,2-hydrogen shift pathway in d⁶ metal complexes.¹⁸ The first ab initio theoretical work of Wakatsuki et al. on the $[\text{Cl}_2\text{Ru}(\text{PH}_3)_2(\text{HC}\equiv\text{CH})]^+$ complex^{18b} showed that for the acetylene–vinylidene rearrangement in this ruthenium(II) d⁶ complex the 1,2-hydrogen shift path is kinetically favored and indicated that it occurs through a preliminary slippage process to an intermediate species showing an agostic interaction between the metal center and one C–H bond, which then undergoes the 1,2-hydrogen shift of the coordinated hydrogen (path 1B), rather than through a direct 1,2-hydrogen shift of the C≡C coordinated acetylene (path 1A). A stationary state corresponding to the hypothetical hydrido alkynyl intermediate $[\text{Cl}_2(\text{PH}_3)_2\text{Ru}(\text{H})(\text{C}\equiv\text{CH})]^+$ was localized (path 2), but it was found to be very unstable so that the oxidative addition of acetylene is thermodynamically very unfavorable, and path 2 was ruled out. These results have then been confirmed by more recent DFT calculations on the alkyne to vinylidene isomerization of several Ru(II) systems, such as $[\text{Ru}(\text{HC}\equiv\text{CH})(\text{CO})(\text{PH}_3)(\eta^5\text{-C}_9\text{H}_7)]^+$ and $[\text{Ru}(\text{HC}\equiv\text{CH})(\text{PH}_3)_2(\eta^5\text{-C}_9\text{H}_7)]^+$.^{18f} In particular our recent calculations on the $\text{Mn}(\text{HC}\equiv\text{CH})(\text{CO})_2(\text{Cp})$ and $[\text{Ru}(\text{HC}\equiv\text{CR})(\text{PMe}_3)_2(\text{Cp})]^+$ ($\text{R} = \text{H}, \text{Me}$) complexes^{18g,h} showed that the

most favorable path for the alkyne rearrangement on these Mn(I) and Ru(II) d⁶ fragments is the 1,2-hydrogen shift occurring via a preliminary slippage process to an agostic intermediate (path 1B) with an overall energy barrier of 19–27 kcal mol⁻¹, while the oxidative addition path shows higher energy barriers, 29–35 kcal mol⁻¹ for the alkyne oxidative addition step and 45–50 kcal mol⁻¹ for the following 1,3-hydrogen shift. Moreover, our BPW91/6-311G**//BPW91/6-31G** calculations on the [Ru(HC≡CMe)-(PMe₃)₂(Cp)]⁺ complex lead to a good agreement between the calculated and experimental activation enthalpy of the alkyne to vinylidene isomerization, showing that this level of calculation is able to reproduce the experimental behavior of such metal-assisted alkyne rearrangement processes.^{18h}

3. Computational Details

All calculations were performed with the Jaguar 7.5 quantum chemistry package,³⁰ using density functional theory (DFT) with the B3LYP hybrid functional,³¹ which is known to give good descriptions of reaction profiles for transition-metal-containing compounds.³² Moreover, the consistency of the energetics of B3LYP and other functionals with MP2 results has been checked by us in a recent computational study on the acetylene and propyne to vinylidene isomerization on the $[(\eta^5-C_5H_5)Ru(PMe_3)_2]^+$ metal fragment and shown to provide activation parameters in good agreement with experimental data.^{18h} We also employed the PBE functional,³³ which has been recently shown to perform as the best, among the common hybrid and gradient-corrected functionals, in predicting the energy difference of cumulene and polyyne isomers,³⁴ the same change involved in the considered isomerization. The 1s–4d core electrons of the ruthenium atom were described with the Hay and Wadt core–valence relativistic effective core potential (ECP),³⁵ leaving the outer electrons to be treated explicitly by a basis set of double- ζ quality and two polarization sp functions, while all electrons were considered for remaining atoms with the 6-31G(d,p) basis set³⁶ (denoted as LACVP** in Jaguar). All structures were optimized in the gas phase with this basis set using both B3LYP and PBE functionals, and frequency calculations were performed to verify the correct nature of the stationary points and to estimate zero-point energy (ZPE) and vibrational entropy corrections at room temperature and calculate the enthalpy and free energy values. Intrinsic reaction coordinate (IRC) calculations were employed to correctly locate reagents and products. Solvation energies were evaluated by using the Poisson–Boltzmann (PB) continuum solvent method³⁷ implemented in Jaguar³⁸ to simulate the THF

Chart 2. Most Stable Isomers of the Metal-Coordinated C₄H₂ Moiety, with Main Bond Distances (Å)



environment employed in nearly all the experimental studies. For all the species involved in intramolecular rearrangements, solvation energies were only evaluated on the gas-phase stationary points, whereas for the proton dissociation and migration processes geometry optimizations and transition state searches were performed in solution starting, whenever possible, from the gas-phase geometries. The electronic and solvation energies of all stationary points have been reevaluated with single-point calculations using the larger LACV3P++*, consisting of the 6-311++G(d,p) set for the main-group elements,³⁹ and of the Hay and Wadt core valence ECP basis set of triple- ζ quality plus one diffuse d function and two polarization sp functions for the metal atom.³⁵ The chemically more interesting reaction or activation enthalpy values in solution at the PB-B3LYP/LACV3P++*/B3LYP/LACVP** level (PB-B3LYP/LACV3P++*/PB-B3LYP/LACVP** for the proton migration processes) will be used in the discussion, and corresponding free energy values will be given in parentheses or cited whenever appropriate. The corresponding PBE values differ by less than 1–3 kcal mol⁻¹ and have only been reported in the Supporting Information (Table S1).

Since the correct evaluation of the proton dissociation and migration processes and the accurate prediction of pK_a values are difficult and challenging tasks, we performed these calculations including a few explicit THF molecules in the first solvation shell of the proton and of the protonated and deprotonated species (see below for more details).

pK_a values were calculated using the equation

$$pK_a = - \frac{\Delta G}{2.303RT} \quad (1)$$

(39) Frisch, M. J.; Pople, J. A.; Binkley, J. S. *J. Chem. Phys.* **1984**, 80, 3265.

- (30) *Jaguar 7.5*; Schrodinger, Inc., Portland, OR, 2008.
- (31) (a) Becke, A. D. *J. Chem. Phys.* **1993**, 98, 5648. (b) Lee, C. T.; Yang, W. T.; Parr, R. G. *Phys. Rev. B* **1988**, 37, 785.
- (32) (a) Paier, J.; Marsman, M.; Kresse, G. *J. Chem. Phys.* **2007**, 127, 024103. (b) Harvey, J. N. *Annu. Rep. Prog. Chem., Sect. C* **2006**, 102, 203.
- (c) Sousa, S. F.; Fernandes, P. A.; Ramos, M. J. *J. Phys. Chem. A* **2007**, 111, 10439. (d) Furche, F.; Perdew, J. P. *J. Chem. Phys.* **2006**, 124, 044103.
- (33) Perdew, J. P.; Burke, K.; Enzerhof, M. *Phys. Rev. Lett.* **1996**, 67, 3865.
- (34) Zhao, Y.; Truhlar, D. G. *J. Chem. Phys.* **2006**, 125, 194101.
- (35) (a) Hay, P. J.; Wadt, W. R. *J. Chem. Phys.* **1985**, 82, 270. (b) Wadt, W. R.; Hay, P. J. *J. Chem. Phys.* **1985**, 82, 284. (c) Hay, P. J.; Wadt, W. R. *J. Chem. Phys.* **1985**, 82, 299.
- (36) Ditchfield, R.; Herhe, W. J.; Pople, J. A. *J. Comput. Chem.* **1971**, 54, 724.
- (37) (a) Tomasi, J.; Persico, M. *Chem. Rev.* **1994**, 94, 2027. (b) Cramer, C. J.; Truhlar, D. G. *Chem. Rev.* **1999**, 99, 2161.
- (38) (a) Tannor, D. J.; Marten, B.; Murphy, R. B.; Friesner, R. A.; Sitkoff, D.; Nicholls, A.; Ringnalda, M. N.; Goddard, W. A., III; Honig, B. *J. Am. Chem. Soc.* **1994**, 116, 11875. (b) Marten, B.; Kim, K.; Cortis, C.; Friesner, R. A.; Murphy, R. B.; Ringnalda, M. N.; Sitkoff, D.; Honig, B. *J. Phys. Chem.* **1996**, 100, 11775.

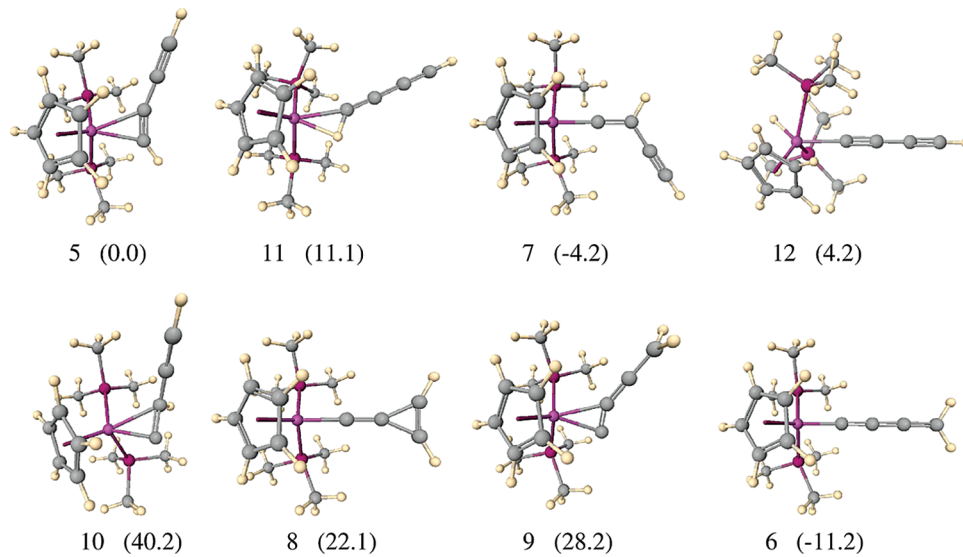


Figure 1. Optimized geometries of the main minima on the potential energy surface for C_4H_2 coordinated to the $[(\text{Cp})(\text{PMe}_3)_2\text{Ru}]^+$ fragment. Relative energies (kcal mol^{-1}) with respect to **5** are reported in parentheses.

where ΔG is the free energy in solution for the considered deprotonation process.

4. Results

Geometries and Stabilities of the Metal Butadiyne Isomers.

We started our analysis by searching for the main equilibrium structures on the potential energy surfaces of the C_4H_2 unit bound to the $[\text{Ru}(\text{PMe}_3)_2(\text{Cp})]^+$ metal fragment, along all the considered isomerization pathways in Scheme 4.

We have found altogether six minima, corresponding to different binding modes of the C_4H_2 isomers **1–4**: i.e., the η^2 -butadiyne complex **5**, the η^1 -butatrienylidene complex **6**, the η^1 -ethynylvinylidene complex **7**, the cyclopropenylidene carbene complex **8**, and the η^2 -bound butatrienylidene and ethynylvinylidene complexes **9** and **10** (see Chart 2, where main bond distances are also reported; the corresponding geometries are shown in Figure 1, whereas the main bond distances and angles are reported in Tables S2 and S3 (Supporting Information)).

Because of their high reactivity, no X-ray structure is available for any of the considered species. However, our previous calculations on the analogous methyl vinylidene complex with the same ruthenium fragment, $[\text{Ru}(=\text{C}=\text{CMe})(\text{PMe}_3)_2(\text{Cp})]^+$,^{18h} have shown that the present level of theory gives a geometry in excellent agreement with the X-ray experimental data for the $[(\text{Cp})(\text{PMe}_3)_2\text{Ru}(=\text{C}=\text{CMe})]^+[\text{PF}_6^-]$ species,^{16a} with deviations almost within experimental uncertainty.

The results for the relative enthalpies (see Table 1) indicate that the coordination to this Ru(II) d^6 metal center considerably changes the energy order of the free C_4H_2 isomers **1–4**, the presence of a low-lying empty d_σ orbital and high-lying filled d_π orbitals on Ru stabilizing the η^1 -bound carbene structures **2–4**, and we found the butatrienylidene complex **6** as the global minimum. This result is consistent with the experimental studies indicating that this species rapidly forms upon the addition of butadiyne to the $[(\text{Cp})(\text{PMe}_3)_2\text{Ru}(\text{THF})]^+$ synthon, although it could not be observed because of its high reactivity toward nucleophiles.

The butadiyne complex **5** has been found at 11.2 kcal mol^{-1} above **6**, higher than the ethynyl vinylidene complex **7**, which is only 7.0 kcal mol^{-1} above **6**. The cyclopropenyl

Table 1. Relative Electronic Energies, Enthalpies, and Free Energies in the Gas Phase and in Solution and Solvation Free Energies of All Isomers and Transition States of $[\text{Ru}(\text{HC}\equiv\text{CC}\equiv\text{CH})(\text{PMe}_3)_2(\text{Cp})]^+{}^a$

structure	gas phase			solution			
	D_e	H	G	D_e	H	G	ΔG_{solv}
5	0.00	0.00	0.00	0.00	0.00	0.00	-34.6
6	-13.1	-12.8	-14.1	-11.5	-11.2	-12.5	-33.1
7	-3.6	-3.3	-4.8	-4.5	-4.2	-5.7	-35.6
8	20.0	20.0	19.2	22.1	22.1	21.3	-32.5
9	28.5	28.2	27.9	28.4	28.2	27.8	-34.7
10	42.4	42.8	40.4	39.7	40.2	37.8	-37.2
11	12.0	11.0	9.7	12.0	11.1	9.8	-34.6
12	7.2	6.2	5.6	5.2	4.2	3.6	-36.6
TS _{5→11}	17.3	15.0	14.9	19.3	17.0	16.8	-32.7
TS _{5→10}	54.6	51.9	51.6	54.1	51.4	51.1	-35.1
TS _{10→7}	45.4	44.4	44.5	43.7	42.8	42.9	-36.3
TS _{11→7}	24.7	21.8	19.5	26.0	23.1	20.8	-33.3
TS _{11→12}	30.6	29.0	26.0	26.3	24.7	21.7	-39.0
TS _{12→10}	53.6	50.9	48.3	50.6	48.0	45.3	-37.6
TS _{7→6}	56.6	53.1	50.5	57.8	54.3	51.8	-33.4
TS _{5→9}	98.1	93.9	93.5	99.0	94.7	94.3	-33.8
TS _{12→6}	84.7	81.3	80.7	82.9	79.5	79.0	-36.4
TS _{6→8}	54.8	52.5	51.5	55.6	53.3	52.3	-33.8

^a Energies are given in kcal mol^{-1} .

methylene complex **8** has been found to be relatively low in energy, 33.3 kcal mol^{-1} above **6** and 22.1 kcal mol^{-1} above **5**, suggesting a possible role for this unusual species in the butadiyne rearrangement.

In the search for the mechanism of the butadiyne to butatrienylidene isomerization (see below) we also located two further low-energy minima corresponding to the η^2 -C–H coordinated agostic butadiyne complex **11** and the hydrido butadiynyl complex resulting from the oxidative addition of the C–H bond, **12**, which were found respectively to be 22.3 and 15.4 kcal mol^{-1} higher in energy than **6** (see Table 1), and the deprotonated neutral butadiynyl species **13** (see Chart 2).

Butadiyne to Butatrienylidene Rearrangement. We then considered the possible pathways leading to the rearrangement from the butadiyne complex **5**, $[(\text{Cp})(\text{PMe}_3)_2\text{Ru}(\eta^2\text{-HC}\equiv\text{CC}\equiv\text{CH})]^+$, assumed to form initially when

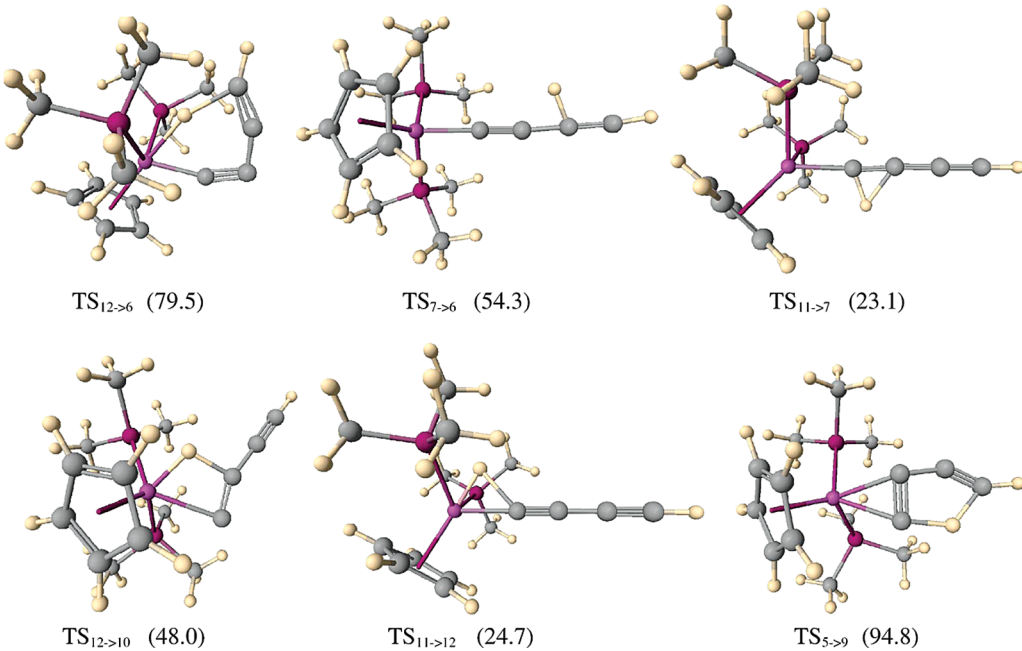


Figure 2. Optimized geometries of the main transition states on the potential energy surface for C_4H_2 coordinated to the $[(\text{Cp})(\text{PMe}_3)_2\text{Ru}]^+$ fragment. Relative energies (kcal mol^{-1}) with respect to **5** are reported in parentheses.

$\text{HC}\equiv\text{CC}\equiv\text{CH}$ is added to the $[(\text{Cp})(\text{PMe}_3)_2\text{Ru}(\text{THF})]^+$ precursor, to the butatrienylidene species **6**, identified as the key intermediate in the formation of new substituted allenylidene and ethynyl complexes.²⁴

On the basis of the structure of the two isomers, and exploiting the analogy with the isomerization of the terminal acetylene to vinylidene, we considered the three possible mechanisms reported in Scheme 4.

Path I: Direct Intramolecular 1,4-Hydrogen Shift. A preliminary energy scan was performed to explore the potential energy surface along the direct 1,4-hydrogen shift from C_α to C_δ in the butadiyne complex **5**, path IA, taking the $\text{C}_\delta-\text{H}$ distance as the reaction coordinate, which was varied from 4.61 Å, the value in **5**, to 1.09 Å, the final value in **6**, obtaining a maximum in the energy profile 97 kcal mol^{-1} above **5**. We then performed a transition state search starting from the structure of the maximum, finding a transition state, $\text{TS}_{5\rightarrow 9}$, 94.8 kcal mol^{-1} in enthalpy above **5**. The frequency analysis gave an imaginary frequency of 1835 cm^{-1} corresponding to the expected normal mode: i.e. the stretching of the breaking $\text{C}_\alpha-\text{H}_\alpha$ and incipient $\text{C}_\delta-\text{H}_\alpha$ bonds.

Subsequent IRC calculations have shown that $\text{TS}_{5\rightarrow 9}$ is connected backward to **5** and forward not to **6** but to its η^2 -bound isomer **9**, 39.3 kcal mol^{-1} higher in energy, 28.2 kcal mol^{-1} above **5**, which is expected to rearrange easily to the most stable η^1 structure **6** with a barrier of few kcal mol^{-1} , as observed for the corresponding rearrangement of the η^2 isomer of the analogous ethynyl vinylidene complex, **10** and **7**, see below. The geometry of $\text{TS}_{5\rightarrow 9}$ (see Figure 2) shows a strong bending of the initially linear butadiyne moiety so to allow both terminal carbon atoms to interact with the shifting hydrogen atom, with $R(\text{C}_\alpha-\text{H}) = 1.522 \text{ \AA}$ and $R(\text{C}_\delta-\text{H}) = 1.487 \text{ \AA}$ (see Figure 2). The large bending of the CCC angles of the sp-hybridized carbon atoms is probably responsible for the high enthalpy barrier of this path, which can therefore be ruled out.

Since for the alkyne to vinylidene isomerization the 1,2-hydrogen shift is known to pass through an η^2 -bound

C–H agostic intermediate, as mentioned above, we also considered the direct 1,4-hydrogen shift to **6** starting from the agostic complex **11**, path IB, and performed a new energy scan, taking again the $\text{C}_\delta-\text{H}$ distance as the reaction coordinate. However, the energy profile shows that along its trajectory from C_α to C_δ the shifting hydrogen atom binds first to the C_β atom, forming the ethynyl vinylidene complex **7**. We therefore did not further analyze this pathway, since it corresponds to the initial step in the two-step mechanism passing through the ethynyl vinylidene species, path II, and is considered below. A comparison of the geometries of the butadiyne unit in **5** and **11** (see Figure 1) indicates the reason for the different behavior observed for the 1,4-hydrogen shift starting from these two complexes: while in **5**, due to the coordination of the $\text{C}_\alpha\equiv\text{C}_\beta$ triple bond, the $\text{C}_\alpha\text{C}_\beta\text{C}_\gamma$ angle is significantly bent (159.7°) and favors the approach of C_α to C_δ required for the direct 1,4-hydrogen shift, in **11** the C_4 chain is almost linear, making the C_α to C_δ approach more difficult and favoring the C_α to C_β approach, i.e. the 1,2-H shift.

Path II: Two-step Pathway through the Ethynyl Vinylidene Intermediate. **(1) Butadiyne to Ethynyl Vinylidene Isomerization.** We addressed the initial 1,2-H shift from **5** to the ethynyl vinylidene complex **7**, considering all the three possible pathways for the 1-alkyne to vinylidene isomerization reported in Scheme 3: i.e. the intramolecular 1,2-hydrogen shift from C_α to C_β with a concomitant detachment of C_β from the metal either directly from the η^2 C–C alkyne complex (path 1A) or passing through a η^2 C–H agostic alkyne intermediate (path 1B) and the oxidative addition of the coordinated 1-alkyne to give a hydrido alkynyl complex which then isomerizes by a 1,3-hydrogen shift from the metal to C_β (path 2).

(i) Path 1A. The optimization of a transition state corresponding to the direct 1,2-hydrogen shift in the coordinated butadiyne complex **5** led to the structure $\text{TS}_{5\rightarrow 10}$, actually connected with the unstable η^2 -bound ethynyl vinylidene complex **10**, as checked by an IRC analysis, 51.4 kcal mol^{-1} above **5**. We could also locate the transition state, $\text{TS}_{10\rightarrow 7}$,

corresponding to the conversion of the η^2 -bound ethynyl vinylidene complex **10** to the most stable η^1 -bound isomer **7**, finding it only 2.6 kcal mol⁻¹ above **10**.

(ii) Path 1B. We first considered the initial slippage process from the butadiyne η^2 -C–C complex **5** to the corresponding η^2 -C–H agostic species, **11**, which was found only 11.1 kcal mol⁻¹ above **5**. A transition state, **TS_{5→11}**, could be optimized 17.0 kcal mol⁻¹ above **5**, suggesting that the η^2 -C–C to η^2 -C–H slippage is a quite easy process. We then looked for the transition state for the 1,2-hydrogen shift from **11** to the ethynyl vinylidene complex **7**, finding a structure, **TS_{11→7}**, 12.0 kcal mol⁻¹ higher than **11** and therefore 23.1 kcal mol⁻¹ above **5** in enthalpy (23.1 kcal mol⁻¹ in free energy).

(iii) Path 2. We then considered the oxidative addition process from the already characterized agostic complex **11** to the relatively low energy hydrido butadiynyl complex **12** (only 4.2 kcal mol⁻¹ above **5**) and optimized the transition state, **TS_{11→12}**, 13.6 kcal mol⁻¹ above **11** and 24.7 kcal mol⁻¹ above **5**. We then searched for the transition state of the 1,3-hydrogen shift from the metal to C_β and found a structure, **TS_{12→10}**, 43.7 kcal mol⁻¹ above **12** and therefore 48.0 kcal mol⁻¹ above **5**, which was shown by IRC calculations to connect **12** to the η^2 -ethynyl vinylidene complex **10**, which then easily relaxes to the more stable η^2 isomer **7** through the negligibly small barrier of 2.6 kcal mol⁻¹ already calculated within path 1B (see above).

A schematic representation of the potential energy surface for the overall 1,2-hydrogen shift in path 1A, 1B, and 2 has been reported in Figure 3 and shows that the lowest enthalpy barrier to the formation of the ethynyl vinylidene complex **7**, 23.1 kcal mol⁻¹ (20.2 kcal mol⁻¹ in free energy), is observed for path 1B, whereas paths 1A and 2 show much higher enthalpy barriers at 51.4 and 48.0 kcal mol⁻¹, respectively.

We hereby note that, although the high enthalpy barrier for the intramolecular 1,3-hydrogen shift, 48.0 kcal mol⁻¹, allows us to rule out the formation of the ethynyl vinylidene complex **7** through the oxidative addition path, the oxidative addition reaction has a moderately high barrier (24.7 kcal mol⁻¹) and the formation of the relatively stable hydrido butadiynyl complex **12** (4.2 kcal mol⁻¹ above **5**) might become a competitive process in the butadiyne rearrangement on this electron-rich fragment.

(2) Ethynyl Vinylidene to Butatrienylidene Isomerization. Two different kinds of pathways can be envisaged for the shift of the vinylidenic hydrogen from the C_β to the terminal C_δ atom, leading from the ethynyl vinylidene intermediate to the final butatrienylidene complex: (i) an intramolecular hydrogen shift, either through a direct 1,3-H shift or two subsequent 1,2-shifts, first from C_β to C_γ and then from C_γ to C_δ (path IIA) and (ii) a proton migration process occurring through the deprotonation at C_β of the ethynyl vinylidene **7** leading to the butadiynyl complex **13**, which is then reprotonated at C_δ to give the final butatrienylidene product **6** (path IIB) (see Scheme 4). Both pathways will be addressed in detail below.

(i) Intramolecular Pathway (IIA). We first considered the two-step process occurring through two consecutive 1,2-H shifts first from C_β to C_γ and then from C_γ to C_δ . A preliminary geometry optimization was performed on the hypothetical isomer with one hydrogen atom bound to the C_γ and one to the C_δ atom. Although we started from several plausible initial geometries, no minima corresponding to this structure were obtained and the geometry optimization led

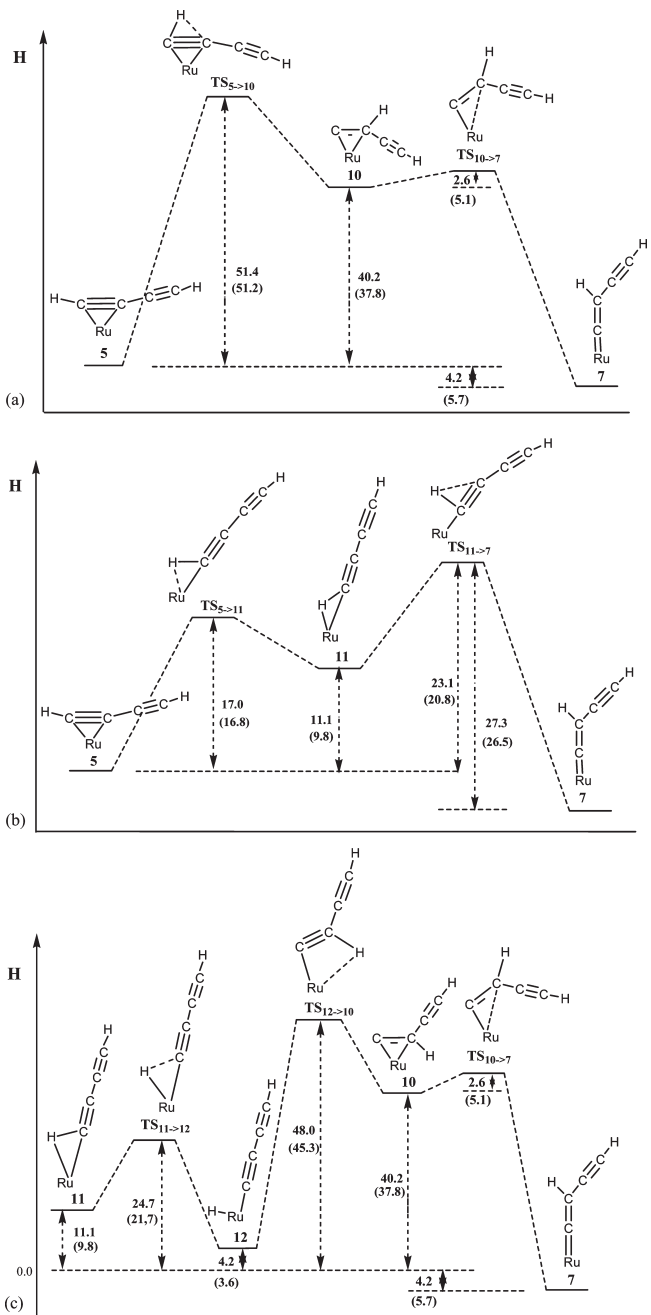


Figure 3. Schematic enthalpy profile calculated for the three considered pathways for the η^2 -alkyne \rightarrow η^1 -vinylidene isomerization: (a) pathway 1A; (b) pathway 1B; (c) pathway 2. Data in parentheses refer to the corresponding free energy values. Energies are in kcal mol⁻¹.

either to the ethynyl vinylidene or the butatrienylidene isomer, depending on the initial geometry. We therefore ruled out this two-step pathway and considered only the direct 1,3-hydrogen shift. A preliminary energy scan was performed to explore the potential energy surface along this direction, taking the C_δ –H distance as the reaction coordinate, which was varied from 3.30 Å, the value in **7**, to 1.07 Å, the final value in **6**, giving a maximum in the energy profile ca. 61 kcal mol⁻¹ above **7**. We then performed a transition state search starting from the structure of the maximum and found a transition state, **TS_{7→6}**, 58.5 kcal mol⁻¹ in enthalpy above **7** and 54.3 kcal mol⁻¹ above **5**. The frequency analysis

gave an immaginary frequency of 1057 cm^{-1} corresponding to the expected normal mode. Subsequent IRC calculations have confirmed that **TS₇₋₆** is connected backward to **7** and forward to **6**. The geometry of **TS₇₋₆** (see Figure 2) shows that the hydrogen atom is between the C_{β} and C_{γ} atoms and is closer to the latter, with $R(C_{\beta}-\text{H}) = 1.522\text{ \AA}$ and $R(C_{\gamma}-\text{H}) = 1.188\text{ \AA}$. The relatively large bending of the CCC angles of the sp-hybridized C_{γ} atom and the instability of the intermediate structure with the hydrogen bound to the C_{γ} atom are probably responsible for the quite high enthalpy barrier of this intramolecular pathway, which cannot explain the easy isomerization observed at room temperature and can therefore be ruled out.

While investigating the potential energy surface along the **7** to **6** rearrangement, we found a relatively stable structure corresponding to the cyclopropenylidene carbene complex **8** only $22.1\text{ kcal mol}^{-1}$ above the butadiyne complex **5**, which could therefore be a possible metastable species, provided that the barriers for its rearrangement to **6** or **7** were high enough. We have therefore considered the possible pathways for the isomerization from **8** to **6** and to **7** and, after preliminary energy scans, we were able to optimize the corresponding transition states, **TS₈₋₆** and **TS₈₋₇**, respectively 31.2 and $43.1\text{ kcal mol}^{-1}$ in enthalpy above **8**. Although these barriers are large enough to suggest that **8** could be detected as a metastable species even at room temperature, the high activation enthalpy for its formation from **6** or **7**, respectively 64.5 and $69.4\text{ kcal mol}^{-1}$, indicates that this species cannot be formed at room or slightly higher temperatures.

(ii) Proton Transfer Pathway (IIB). Since metal vinylidenes are known to be relatively strong acids (for instance, a value of 7.74 has been measured for the $\text{p}K_{\text{a}}$ of the $[\text{Ru}(=\text{C}=\text{CHMe})(\text{dppe})\text{Cp}]^+$ complex in 2:1 THF–water⁴⁰), once the ethynyl vinylidene complex is formed, the deprotonation of the C_{β} -bound hydrogen is expected to be a plausible process. A proton migration mechanism can therefore be hypothesized, proceeding by a sequential proton dissociation from the ruthenium ethynyl vinylidene species **7** to yield the neutral butadiynyl complex **13** and its protonation at the terminal butadiynyl C_{δ} carbon atom leading to the final butatrienyldiene complex (path IIB in Scheme 4).

A reliable prediction of the energy profile for this proton migration process requires an accurate evaluation of the solvation free energy of all the charged species involved and, in particular, of the small proton species H^+ . Unfortunately continuum solvation methods do not properly account for short-range intermolecular interactions, such as ion–dipole and hydrogen bonding, which are considered to be particularly important in the solvation of charged molecules.⁴¹ Several studies have recently shown that the inclusion of a few explicit solvent molecules improves the accuracy of the calculated solvation free energies.⁴² In particular, this explicit–implicit solvation approach has been applied to the calculation of the $\text{p}K_{\text{a}}$ of several weak

(40) Davidson, A.; Selegue, J. P. *J. Am. Chem. Soc.* **1978**, *100*, 7763.
(41) (a) Camaioni, D. M.; Dupuis, M.; Bentley, J. *J. Phys. Chem. A* **2003**, *107*, 5778. (b) Chipman, D. M.; Chen, F. *J. Chem. Phys.* **2006**, *124*, 144507.

(42) (a) Pliego, J. R., Jr.; Riveros, J. M. *J. Phys. Chem. A* **2001**, *105*, 7241. (b) Kelly, C. P.; Cramer, C. J.; Truhlar, D. G. *J. Chem. Theor. Comput.* **2005**, *1*, 1133. (c) Kelly, C. P.; Cramer, C. J.; Truhlar, D. G. *J. Phys. Chem. B* **2006**, *110*, 16066. (d) Ahlquist, M.; Kozuch, S.; Shaik, S.; Tanner, D.; Norrby, P. O. *Organometallics* **2006**, *25*, 45. (e) Vyacheslav, S.; Bryantsev, V. S.; Diallo, M. S.; Goddard, W. A., III *J. Phys. Chem. B* **2008**, *112*, 9709.

Scheme 5. Thermodynamic Cycle for the Calculation of $\Delta G_{\text{solv}}^*(\text{H}^+)$

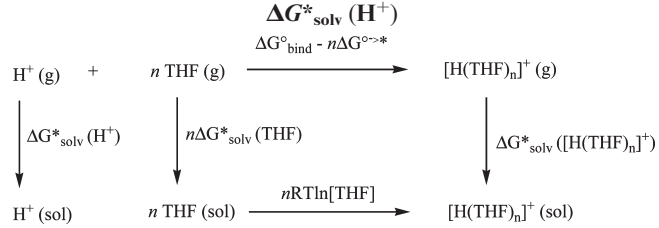


Table 2. $\Delta G_{\text{solv}}^*(\text{H}^+)$ Calculated with the Pure PB Continuum Solvent Approach ($n = 0$) and Including from One to Four Explicit THF Molecules ($n = 1-4$) (See Text)^a

n	$\Delta G_{\text{solv}}^*(\text{H}^+)$
0	-125.0
1	-248.3
2	-256.8
3	-252.0
4	-247.3
exptl	256–257

^a Energies are given in kcal mol^{-1} .

acids, in both water and nonaqueous solvents, giving results in good agreement with the experimental values.⁴³

To test the reliability of this approach to the deprotonation in THF solution and to determine the optimal number of explicit THF molecules to include in the calculations, we have first calculated the standard solvation free energy of the proton in THF, $\Delta G_{\text{solv}}^*(\text{H}^+)$, employing the thermodynamic cycle in Scheme 5.^{42e} According to this cycle $\Delta G_{\text{solv}}^*(\text{H}^+)$ is given by

$$\Delta G_{\text{solv}}^*(\text{H}^+) = \Delta G_{\text{g, bind}}^* + \Delta G_{\text{solv}}^*([\text{H}(\text{THF})_n]^+) - n\Delta G_{\text{solv}}^*(\text{THF}) - n\Delta G^{\circ\rightarrow*} - nRT \ln[\text{THF}]$$

where $\Delta G_{\text{g, bind}}^*$ is the gas-phase binding energy of n THF molecules to the proton, $\Delta G_{\text{solv}}^*([\text{H}(\text{THF})_n]^+)$ is the solvation free energy of the $[\text{H}(\text{THF})_n]^+$ cluster, and $\Delta G_{\text{solv}}^*(\text{THF})$ the solvation free energy of THF. Here the symbols “ $*$ ” and “ \circ ” refer to the standard states of 1 mol L^{-1} and 1 atm , respectively, and $\Delta G^{\circ\rightarrow*} = RT \ln(RT)$ is the conversion factor.

$\Delta G_{\text{solv}}^*(\text{H}^+)$ has then been calculated employing from one to four explicit THF molecules ($n = 1-4$), and the results have been compared with the best available experimental value of $256-257\text{ kcal mol}^{-1}$.⁴⁴

The calculated values are reported in Table 2 together with the value obtained from the purely implicit PB approach ($n = 0$) and exhibits a minimum for $n = 2$, with a value of $256.8\text{ kcal mol}^{-1}$, very close to the experimental data. Notice that the PB approach without any explicit THF molecule leads to a huge error of ca. 130 kcal mol^{-1} , and its use in the simulation of the proton migration process would lead to an

(43) (a) Pliego, J. R., Jr.; Riveros, J. M. *J. Phys. Chem. A* **2002**, *106*, 7434. (b) Kelly, C. P.; Cramer, C. J.; Truhlar, D. G. *J. Phys. Chem. A* **2006**, *110*, 2493. (c) Ho, J.; Coote, M. L. *J. Chem. Theor. Comput.* **2009**, *5*, 295. (d) Fu, Y.; Liu, L.; Li, R.-Q.; Liu, R.; Guo, Q.-X. *J. Am. Chem. Soc.* **2004**, *126*, 814. (e) Ding, F.; Smith, J. M.; Wang, H. *J. Org. Chem.* **2009**, *74*, 2679.

(44) This value is obtained by adding to the most recent value of $-265.9\text{ kcal mol}^{-1}$ for $\Delta G_{\text{solv}}^*(\text{H}^+)$ in water estimated by Tissandier et al. (Tissandier, M. D.; Cowen, K. A.; Feng, W. Y.; Gundlach, E.; Cohen, M. H.; Earhart, A. D.; Coe, J. V. *J. Phys. Chem. A* **1998**, *102*, 7787. Camaioni, D. M.; Schwerdtfeger, C. A. *J. Phys. Chem. A* **2005**, *109*, 10795) the value of $+9.6\text{ kcal mol}^{-1}$ estimated for the standard molar free energy of transfer of H^+ from water to pure THF (Markus, Y. *Pure Appl. Chem.* **1983**, *55*, 977 and references therein).

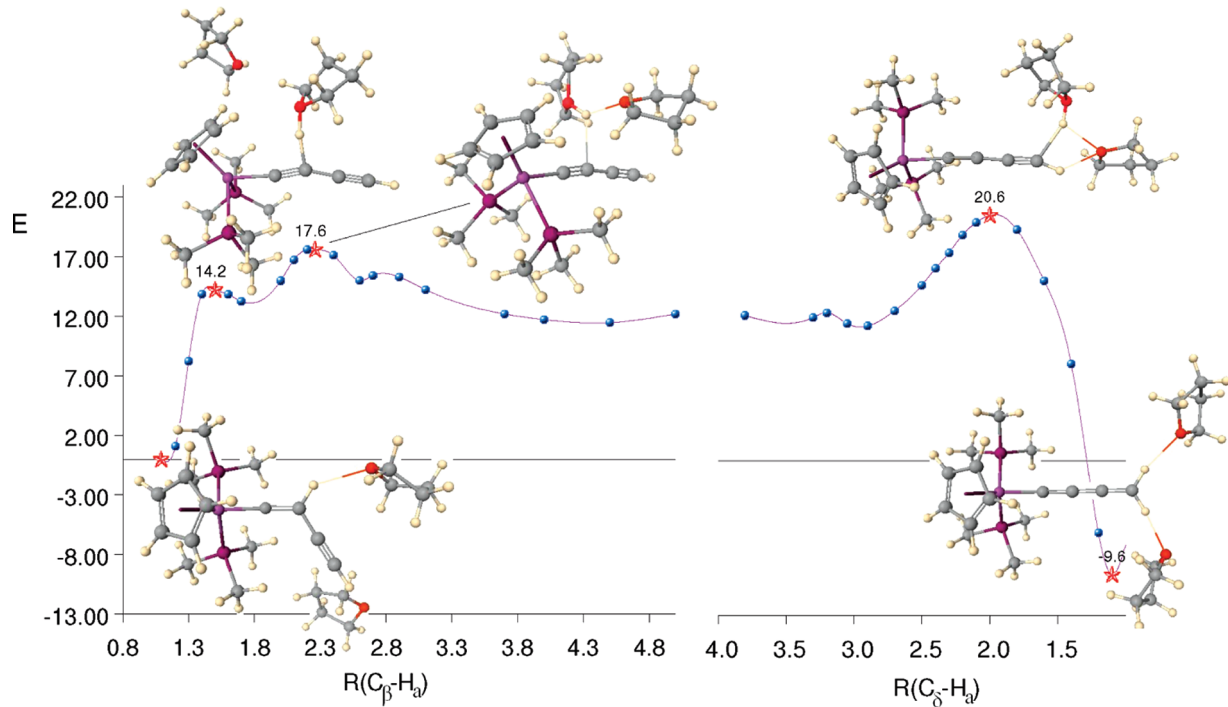
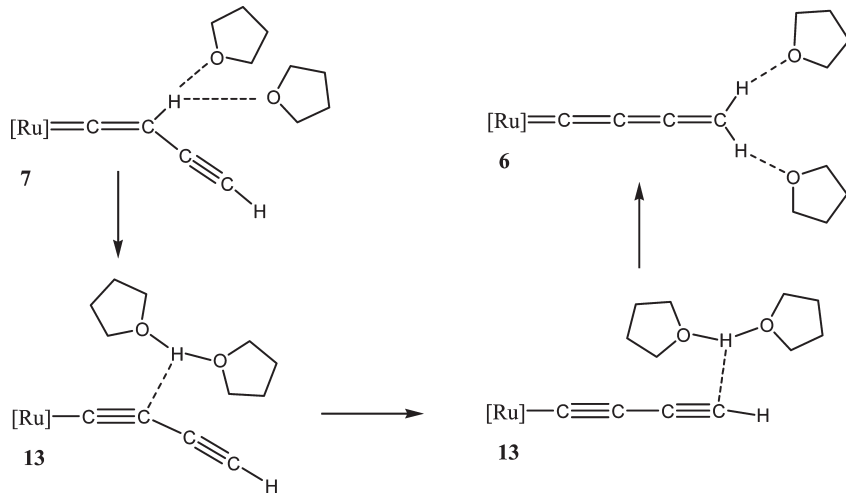


Figure 4. Potential energy curves for the proton migration from the C_β to the C_δ atom in the ethynyl vinylidene complex **7**. On the left is reported the curve for the proton detachment from C_β , taking the C_β -H distance as the reaction coordinate; on the right is shown the curve for the proton approach to C_δ , taking the C_δ -H distance as the reaction coordinate. Energies are given in kcal mol^{-1} .

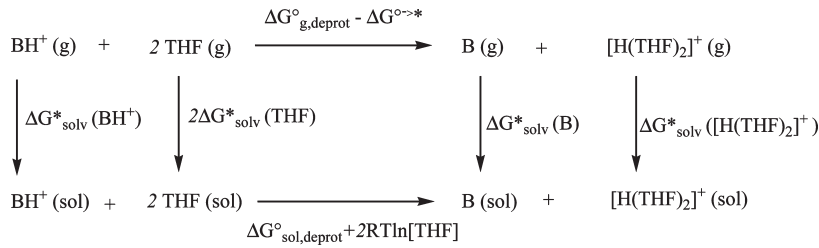
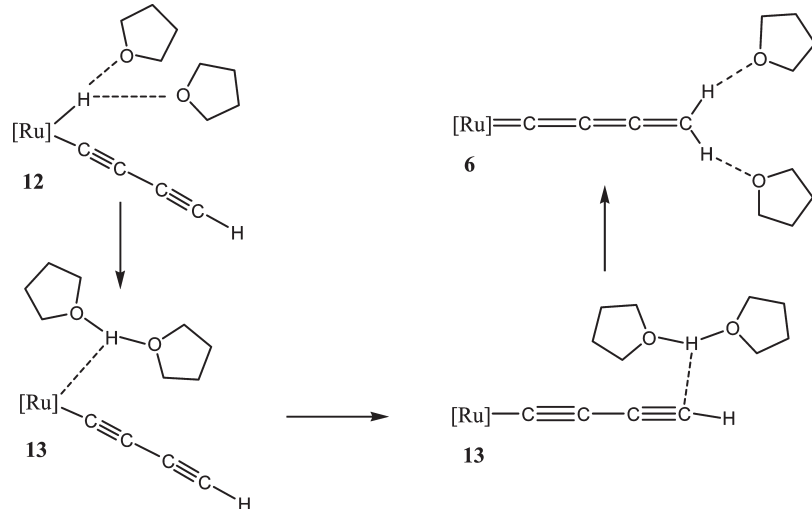
Scheme 6. Proposed Pathway for the Proton Migration from the C_β to the C_δ Atom in the Ethynyl Vinylidene Complex **7 Assisted by Two THF Molecules**



unacceptable inaccuracy. According to the criterion suggested by Pliego et al.^{42a} the ideal number of explicit solvent molecules is that which minimizes the free energy of solvation; thus, we decided to calculate the energy profile for the proton migration from the C_β to the C_δ atom, including two explicit THF molecules according to the pathway in Scheme 6. The optimized geometry of the initial adduct of **7** with two THF molecules shows that one THF molecule forms a hydrogen bond with the vinylidene hydrogen atom, with a $(C_\beta)\text{H} \cdots \text{O}(\text{THF})$ distance of 2.38 Å, while the second THF molecule cannot form another hydrogen bond due to the steric hindrance with the methyl groups on the phosphine ligands and remains farther away. The migration starts with a proton transfer from the ethynyl vinylidene

complex to the oxygen atom of the closest THF molecule and the formation of the butadiynyl complex **13**. The proton transfer occurs with the concomitant approach of the second neighboring THF molecule to form a stable $(\text{THF})_2\text{H}^+$ cluster, which remains close to the butadiynyl chain, interacting with the electron-rich C_β atom. Once the vinylidene proton has been abstracted, the reaction continues with the migration of the $(\text{THF})_2\text{H}^+$ unit along the butadiynyl chain and the protonation of the C_δ atom, leading to the final butatrienyldiene complex **6** and two weakly bound THF molecules.

An energy scan was performed to explore the potential energy surface for this deprotonation process by taking the C_β -H distance as the reaction coordinate, which was varied

Scheme 7. Thermodynamic Cycle Employed for the Calculation of pK_a **Scheme 8. Proposed Pathway for the Proton Migration from the Ruthenium to the C_δ Atom in the Hydrido Butadiynyl Complex 12 Assisted by Two THF Molecules**

from 1.1 Å, the value in **7**, to a sufficiently large value of 5 Å. The calculated energy profile is reported in Figure 4 on the left and shows an apparently unusual trend with two maxima, at 1.50 and 2.26 Å, and a further shoulder at 2.7 Å. The first maximum corresponds to proton transfer from C_β to the adjacent THF oxygen, leading to a (THF) H^+ unit still strongly hydrogen bonded to the C_β atom, with $C_\beta - H = 1.50$ Å, while the second maximum corresponds to the detachment of the (THF) H^+ unit from the C_β atom and the shoulder to the approach of the second THF molecule and the formation of the more stable (THF) $_2H^+$ moiety. A very shallow minimum is observed around 4.3 Å, corresponding to the formation of a weak adduct between the (THF) $_2H^+$ cluster and the butadiynyl complex, which is disrupted at larger $C_\beta - H$ distances. On the whole, these calculations indicate that the proton abstraction has a moderate energy cost, 12 kcal mol⁻¹, and takes place with a relatively low energy barrier of 19 kcal mol⁻¹.

To further test the reliability of this approach, we employed the free energy value calculated for the deprotonation of the ethynyl vinylidene complex **7** to estimate the pK_a value and compare the result with the experimental value measured for the analogous $[\text{Ru}(=\text{C}=\text{CHMe})(\text{dppe})\text{Cp}]^+$ complex.

We employed the thermodynamic cycle in Scheme 7 and calculated the pK_a using eq 1 where the free energy of deprotonation in THF solution has been evaluated as

$$\begin{aligned} \Delta G_{\text{sol,deprot}} &= \Delta G^\circ_{\text{g,deprot}} + \Delta G^*_{\text{solv}}(\text{B}) \\ &+ \Delta G^*_{\text{solv}}([\text{H}(\text{THF})_2]^+) - \Delta G^*_{\text{solv}}(\text{BH}^+) \\ &- 2\Delta G^*_{\text{solv}}(\text{THF}) - RT\ln(RT) - 2RT \\ &\quad \ln[\text{THF}] \end{aligned} \quad (2)$$

In Scheme 7 the cationic ethynyl vinylidene complex **7** is referred to as BH^+ , while B can be considered to represent the neutral butadiynyl complex **13**; $\Delta G^\circ_{\text{g,deprot}}$ is the gas-phase deprotonation free energy, and the other terms have been defined above.

We calculated for pK_a a value of 7.8, which is qualitatively consistent with the experimental value of 7.74 measured for the slightly different $[\text{Ru}(=\text{C}=\text{CHMe})(\text{dppe})\text{Cp}]^+$ complex in 2:1 THF–water.

The protonation of the C_δ atom of **13** by the migrating (THF) $_2H^+$ unit has also been investigated by performing an energy scan, taking as the reaction coordinate the $C_\delta - H$ distance, which was varied from 3.80 Å, the value corresponding to the weak adduct between the (THF) $_2H^+$ cluster and the butadiynyl complex **13** (the shallow minimum in the deprotonation energy profile), to 1.1 Å, the value in the final product **6**. The calculated energy profile (see Figure 4 on the right) shows a maximum at 2.00 Å, 20.6 kcal mol⁻¹ above **7**, and a final geometry of the butatrienyldiene complex **6** where the two terminal hydrogen atoms are hydrogen-bonded with the oxygen atoms of the two THF molecules.

Figure 4 reports the energy profile for the whole proton migration from C_β to C_δ and indicates an overall energy barrier of 20.6 kcal mol⁻¹, corresponding to the protonation of the C_δ atom in the butadiynyl complex **13**, slightly higher than the deprotonation barrier probably due to its lower acidity. A subsequent transition state search in solution, starting from the maximum geometry, allowed us to characterize the transition state, TS_{13-6} , very close in geometry and energy to that of the maximum, and to calculate an overall enthalpy barrier of 20.0 kcal mol⁻¹ for the proton migration from C_β to C_δ , which turns out to be the highest barrier for this process.

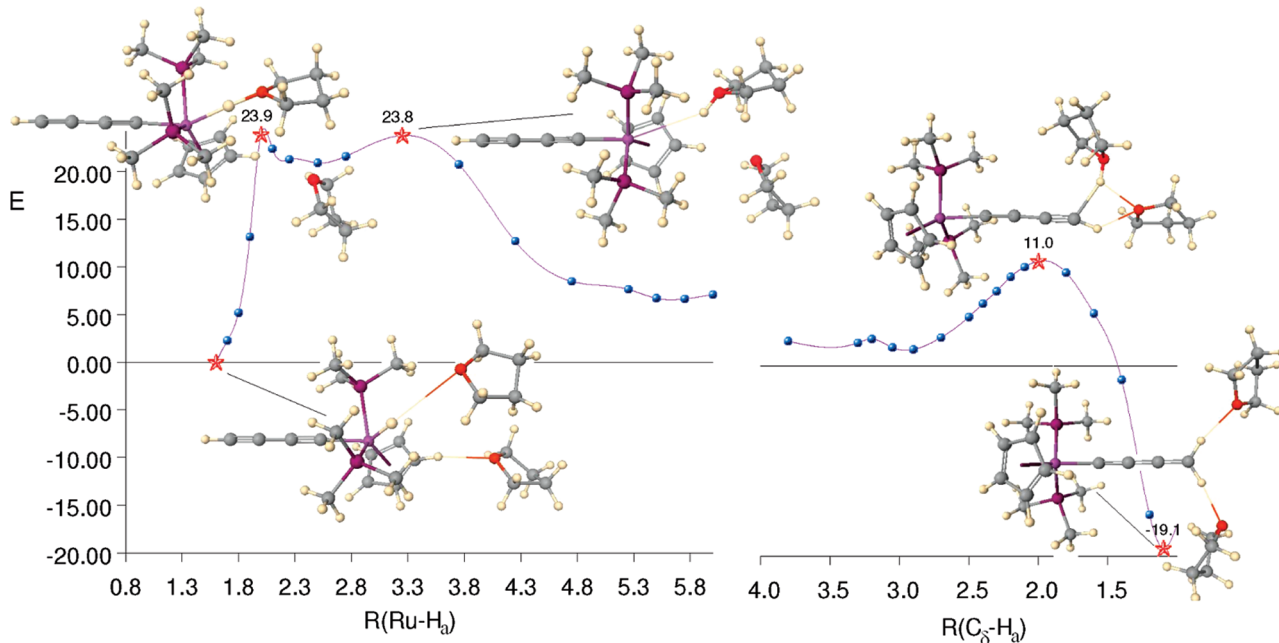


Figure 5. Potential energy curves for the proton migration in the hydrido butadiynyl complex **12** from the Ru to the C_δ atom. On the left is reported the curve for the proton detachment from Ru, taking the Ru–H distance as reaction coordinate; on the right the curve for the proton approach to C_δ , taking the C_δ –H distance as reaction coordinate. Energies are in kcal mol^{-1} .

Such a relatively low energy barrier indicates that this proton migration mechanism from the ethynyl vinylidene complex is an easy process at room temperature and therefore that path IIIB is a plausible mechanism for the butadiyne to butatrienylidene isomerization.

Path III: Oxidative Addition Pathway. (1) Oxidative Addition to the Hydrido Butadiynyl Complex. We have already characterized the oxidative addition of the terminal C–H bond of butadiyne passing through the $\eta^2\text{C–H}$ agostic complex **11**, leading to the hydrido butadiynyl complex **12**, finding that this is a slightly endothermic process (by $4.2 \text{ kcal mol}^{-1}$) with a moderately high enthalpy barrier of $24.7 \text{ kcal mol}^{-1}$ (free energy barrier of $21.7 \text{ kcal mol}^{-1}$), which makes it plausible, although probably slow.

We have also already addressed the isomerization of **12** to the ethynyl vinylidene complex **7** through a 1,3-shift, finding that this is a kinetically unfavorable process with a high activation enthalpy of $48.0 \text{ kcal mol}^{-1}$: we will now consider the isomerization of **12** to the final butatrienylidene complex.

(2) Hydrido Butadiynyl to Butatrienylidene Isomerization. Two different kinds of pathways can also be proposed for the hydrogen shift from the ruthenium to the terminal C_δ atom, leading from the hydrido butadiynyl intermediate **12** to the final butatrienylidene complex **6**: (i) a direct intramolecular 1,5-hydrogen shift (path IIIA) and (ii) a proton transfer process occurring through deprotonation of the ruthenium center followed by the reprotonation of the butadiynyl intermediate **13** to the final butatrienylidene product (path IIIB). Both pathways will be addressed in detail below.

(i) Intramolecular Pathway (IIIA). We first considered the direct 1,5-hydrogen shift from **12** to the butatrienylidene complex **6**; we located a high-energy transition state, $\text{TS}_{12\rightarrow 6}$, which was shown by the IRC calculations to be connected backward to **12** and forward to **6**. The geometry of $\text{TS}_{12\rightarrow 6}$ (see Figure 2) shows a strong bending of the initially linear butadiynyl unit necessary to allow the terminal carbon atom to interact with the shifting hydride ligand, with

$R(\text{Ru–H}) = 1.93 \text{ \AA}$ and $R(C_\delta\text{–H}) = 1.77 \text{ \AA}$. This large bending is probably responsible for the high enthalpy barrier of this latter step, $75.3 \text{ kcal mol}^{-1}$ above **12** and $79.5 \text{ kcal mol}^{-1}$ above **5**, which allows us to exclude this intramolecular path.

(ii) Proton Transfer Pathway (IIIB). Because ruthenium(II) hydride complexes with cyclopentadienyl and diphosphine ligands are also relatively strong acids, for instance values of pK_a in the range 5–9 have been measured in THF for $[\text{CpRu(L-L)}\text{H}_2]^+$ dihydride complexes, where L-L stands for a bidentate species or two monodentate phosphines,⁴⁵ a proton migration mechanism can be hypothesized also in this case, proceeding by a sequential proton dissociation from the ruthenium ethynyl hydrido butadiynyl complex **12** and yielding the neutral butadiynyl complex **13** and protonation at the terminal butadiynyl C_δ carbon atom leading to the final butatrienylidene complex **6** (path IIIB in Scheme 4).

We therefore calculated the energy profile for the proton migration from Ru to the C_δ atom following the same approach employed for the proton migration in the ethynyl vinylidene complex **7**, i.e. including two explicit THF molecules, according to Scheme 8. The optimized geometry of the initial adduct of **12** with two THF molecules shows that one THF molecule—due to the steric clashes with the cyclopentadienyl and phosphine ligands—cannot approach the hydrido atom to form a hydrogen bond, with a $(\text{RuH})\cdots\text{O}(\text{THF})$ distance of 3.66 \AA , and the second THF molecule stays even farther. The migration starts with a proton transfer from the hydrido butadiynyl complex **12** to the oxygen atom of the closest THF molecule and the formation of the butadiynyl complex **13**. The proton transfer occurs with the concomitant approach of the second neighboring THF molecule to form a stable $(\text{THF})_2\text{H}^+$ cluster which remains close to the complex, trans to the butadiynyl chain and interacting with the electron-rich ruthenium atom. Once

(45) Jia, G.; Morris, R. H. *J. Am. Chem. Soc.* **1991**, *113*, 875.

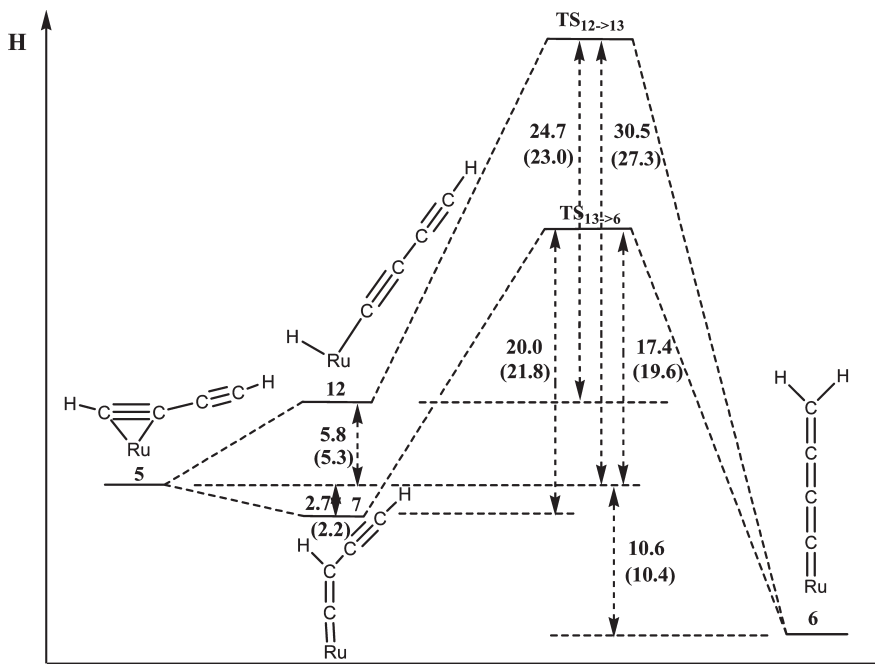


Figure 6. Schematic enthalpy profile of the two lowest pathways calculated for the η^2 -butadiyne \rightarrow η^1 -butatrienylidene isomerization passing through either the ethynyl vinylidene complex **7** or the hydrido butadiynyl complex **12** followed by proton migration from the C_β or the Ru to the C_δ atom. Data in parentheses refer to the corresponding free energy values. Energies are given in kcal mol^{-1} .

the proton has been abstracted from the metal, the reaction continues again with the migration of the $(\text{THF})_2\text{H}^+$ unit and the protonation of the C_δ atom, leading to the final butatrienylidene complex **6** and two weakly bound THF molecules.

An energy scan was performed to explore the potential energy surface for this deprotonation process, taking as the reaction coordinate the Ru–H distance, which was varied from 1.1 Å, the value in **12**, to a sufficiently large value of 6 Å. The calculated energy profile is reported in Figure 5 on the left and shows two maxima, at 2.00 and 3.25 Å. The first maximum corresponds to proton transfer from Ru to the neighboring THF oxygen, leading to a $(\text{THF})\text{H}^+$ unit still hydrogen-bonded to the Ru atom, while the second maximum corresponds to the detachment of the $(\text{THF})\text{H}^+$ unit from the Ru atom, with the approach of the second THF molecule and the formation of the more stable $(\text{THF})_2\text{H}^+$ moiety. No minimum is observed in this case, probably due to the higher steric hindrance around the Ru atom, and the energy steadily decreases until a distance of $\text{Ru}-\text{H} = 6.0$ Å is reached. On the whole, the results of this energy scan (see Figure 5) indicate that although the proton abstraction has a small energy cost, 5.6 kcal mol^{-1} , it takes place with a rather high energy barrier of 23.9 kcal mol^{-1} , probably due to the high steric hindrance with cyclopentadienyl and phosphine ligands which forbids the THF molecules to closely approach the hydrido atom.

We employed again the thermodynamic cycle in Scheme 6 and eqs 1 and 2 to evaluate the pK_a value, and we calculated a value of 1.4, which shows that the hydrido ligand in **12** has a relatively strong acid character, consistent with the known behavior of the $[\text{CpRu}(\text{L-L})\text{H}_2]^+$ dihydride complex in THF.

The migration of the $(\text{THF})_2\text{H}^+$ unit and the protonation of the C_δ atom of **13** have already been investigated above: the energy profile as a function of the $C_\delta-\text{H}$ distance is reported on the right of Figure 5, rescaled on the energy of

Table 3. Relative Electronic Energies, Enthalpies and Free Energies of Isomers **5–**7** and **12** and Transition States **TS**_{13–6} and **TS**_{12–13} Calculated Including Two Explicit THF Molecules^a**

structure	D_e	H	G
5	0.00	0.00	0.00
6	-8.94	-10.63	-10.39
7	-1.61	-2.66	-2.18
12	7.13	5.85	5.26
TS _{13–6}	19.54	17.38	19.61
TS _{12–13}	32.26	30.53	27.25

^a Energies are given in kcal mol^{-1} .

12, and shows that the maximum is only 11.0 kcal mol^{-1} above **12**.

Figure 5 reports the energy profile for the whole proton migration from Ru to C_δ and indicates an overall energy barrier of 23.9 kcal mol^{-1} , corresponding to the deprotonation of the ruthenium atom in the initial hydrido butadiynyl complex **12**, slightly higher than the deprotonation barrier of the ethynyl complex **7** in spite of its higher acidity, probably because of the difficulty of the THF solvent molecules in approaching the sterically crowded metal atom and assisting the proton abstraction. A subsequent transition state search in solution starting from the geometry of the highest maximum geometry, corresponding to the proton abstraction from the metal atom, allowed us to characterize a structure, **TS**_{12–13}, very close in geometry and energy to that of the maximum, only 24.7 kcal mol^{-1} in enthalpy above **12** (23 kcal mol^{-1} in free energy), which turns out to be the highest barrier for this process.

Such a relatively low energy barrier indicates that this proton migration mechanism from the hydrido butadiynyl complex is a possible process at room temperature and therefore also path IIIB could be a plausible mechanism for the butadiyne to butatrienylidene isomerization.

5. Discussion

Our calculations have thus shown only two viable isomerization pathways for the final hydrogen shift to the terminal C_δ atom, both involving a proton migration step, either from the C_β or the metal atom, with activation energies of 20.0 and 24.7 kcal mol⁻¹, respectively.

Figure 6 reports a schematic representation of the potential energy surface for the two isomerization mechanisms involving these proton migration steps: i.e. (i) the two-step process with an initial isomerization of the butadiyne **5** to the ethynyl vinylidene complex **7** through a 1,2-hydrogen shift, followed by a proton migration from the C_β to the C_δ atom (path IIB) and (ii) the two-step process involving an initial oxidative addition of the C–H bond in **5** with formation of the hydrido butadiynyl complex **12** followed by the proton migration from the metal to the C_δ atom (path IIIB). This figure shows that, due to the significantly lower energy of the ethynyl vinylidene **7** compared to the hydrido butadiynyl intermediate **12** (by 8.3 kcal mol⁻¹), the overall activation enthalpy from the butadiyne reagent **5** is sensibly lower for pathway IIB than for IIIB, 17.4 vs 30.5 kcal mol⁻¹, indicating that the former is the favored isomerization pathway.

Notice that in this enthalpy diagram the calculations on the initial butadiyne complex **5**, intermediates **7** and **12**, transition states **TS**_{13–6} and **TS**_{12–13}, and butatrienyldiene product **6** have been performed including two explicit THF molecules and reoptimized in solution within the PB approach. However, the relative energies calculated in this way for **5–7** and **12** (see Table 3) differ only slightly from those obtained through the much less demanding single-point PB calculation on the gas-phase optimized geometries, by 1–3 kcal mol⁻¹, showing that the latter approximation allows us to estimate fairly accurately the solvent effects on these quite large complexes.

6. Concluding Remarks

We have investigated the isomerization of the $[(\text{Cp})(\text{PMe}_3)_2\text{Ru}(\eta^2-\text{HC}\equiv\text{CC}\equiv\text{CH})]^+$ butadiyne complex to the $[(\text{Cp})(\text{PMe}_3)_2\text{Ru}(=\text{C}=\text{C}=\text{C}=\text{CH}_2)]^+$ butatrienyldiene tautomer by DFT calculations, addressing the main plausible mechanisms reported in Scheme 4.

We searched for the main equilibrium structures on the potential energy surface of the C₄H₂ unit bound to the $[(\text{Cp})(\text{PMe}_3)_2\text{Ru}]^+$ metal fragment, along all the considered isomerization pathways. Although the butadiyne **1** is the most stable isomer for the free C₄H₂ moiety, with the butatrienyldiene species **2** 50–55 kcal mol⁻¹ above, our results show that the coordination to the considered Ru(II) d⁶ metal center changes the energy order of the free C₄H₂ isomers and we found as the global minimum the butatrienyldiene complex **6**, with the butadiyne complex **5** 11.2 kcal mol⁻¹ above. This result is consistent with the experimental studies indicating that this species rapidly forms upon the addition of butadiyne to the $[(\text{Cp})(\text{PMe}_3)_2\text{Ru}(\text{THF})]^+$ synthon, although it could not be observed because, due to its high reactivity toward nucleophiles, it reacts immediately with any added nucleophile or even with the solvent, leading to new allenylidenes.

We also characterized the main transition states connecting the calculated minima and evaluated the activation energy of all the considered pathways. Our findings showed that only pathways IIB and IIIB, with the second step proceeding through proton migration, are viable processes with activation enthalpies within 31 kcal mol⁻¹, whereas all the direct hydrogen shifts involving C_δ as the final migration target are very high in energy, above 50 kcal mol⁻¹.

Our calculations provide consistent predictions for a likely isomerization mechanism. The lowest energy path corresponds to a two-step process with an initial isomerization of the butadiyne **5** to the ethynyl vinylidene complex **7** through a 1,3-hydrogen shift followed by a proton migration from the C_β to the C_δ atom (path IIB), for which activation enthalpies of 23.1 and 17.4 kcal mol⁻¹, respectively (activation free energies of 20.8 and 19.6 kcal mol⁻¹), were found.

Acknowledgment. We thank the Italian Ministry for University and Research for financial support (Contract 2006038520).

Supporting Information Available: Tables giving PBE relative energies of all considered minima and transition states, the main bonding distances and bonding angles, and the Cartesian coordinates for the B3LYP optimized geometries. This material is available free of charge via the Internet at <http://pubs.acs.org>.